Dissipative three-wave structures in stimulated backscattering. II. Superluminous and subluminous solitons

Carlos Montes,* Antonio Picozzi, and Derradji Bahloul
Laboratoire de Physique de la Matière Condensée, Centre National de la Recherche Scientifique, Université de Nice–Sophia Antipolis, Parc Valrose, F-06108 Nice Cedex 2, France
(Received 21 June 1996)

Stimulated Brillouin or Raman backscattering of a cw pump into dissipative material and Stokes waves, governed by the nonlinear space-time three-wave resonant model, gives rise to solitary pulses, which are experimentally obtained in long fiber-ring cavities. We show that the known superluminous symmetrical soliton solution is unstable for small dissipation, cascading to a turbulent multipeak structure. A stable single-peak dissipative soliton solution prevails for moderate dissipation (damping), and at a lower critical dissipation operates a pitchfork bifurcation, first yielding a stable bisolitary structure, and then multipeak space-time-dependent structures. Besides a continuous set of asymptotically stable superluminous and subluminous dissipative solitary attractors, the general nonsymmetrical and nonintegrable case is dependent only on the wave front exponential slope of the backscattered Stokes wave, in agreement with the solitary pulses observed in a Brillouin fiber-ring laser. These three-wave dissipative solitons result from the dynamical compensation between the wave-front slope dispersion and the pump depletion. We give an explicit solution for the particular integrable luminous velocity case. We also show that initial steep Stokes envelopes (like Gaussian profiles) evolve to the universal subluminous solitary attractor of paper I. [S1063-651X(97)13301-3]

PACS number(s): 42.81.Dp, 42.65.Es, 42.65.Dr, 42.65.Tg

I. INTRODUCTION

Stimulated Brillouin backscattering (SBBS) experiments in liquids [1], gases [2], plasmas [3], and in fiber-ring resonators [4–6], and stimulated Raman backscattering (SRBS) in liquids [7,8], give rise to localized traveling backscattered Stokes pulses. The space-time dynamics in one spatial dimension, resulting from the resonant three-wave nonlinear interaction between the pump wave E_p, the material wave E_a, and the backscattered Stokes wave E_S, is governed by the nonlinear three-wave partial differential equations (PDE) model within the slowly varying envelope approximation. This model is particularly appropriate for describing the dynamics in single-mode optical fibers [9,4]. The three-wave interaction problem has been the object of many theoretical studies and numerical simulations, to which we referred in paper I [10].

We are interested in nonconservative SBBS or SRBS in the presence of a continuous pump, which has been integrated by the inverse scattering transform (IST) in the nondissipative case [11], giving rise to backscattered solitons. Our aim here is to study the nonconservative problem in the presence of material and Stokes dissipation (damping), in order to analyze the nonlinear dynamics in a cw-pumped optical-fiber-ring laser, where the periodic round-trip interaction in a long lossy cavity may be associated with the nonconservative unlimited interaction. Indeed, it has been shown in a Brillouin fiber-ring cavity that, above the laser threshold and below a critical feedback, generation of dissipative solitary SBBS Stokes pulses [5] takes place from any initial condition [6].

The main purpose here is to present for this problem a continuous family of dissipative solitary attractors resulting from the unlimited three-wave interaction of the cw pump in the presence of dissipative Stokes and material waves. The dissipation then introduces the concept of an attractor, yielding solitary structures extremely robust with respect, for instance, to noise perturbations. These attractors support the experimental observation of a large variety of dissipative solitary Stokes pulses in a Brillouin fiber-ring cavity, among them the experimental results presented here.

From a theoretical point of view, two kinds of initial and/or boundary conditions for the E_a or E_S envelopes will yield two classes of localized traveling backscattered structures.

(I) It was shown in paper I [10] that the cw pump interacting with initially *bounded* Stokes or material wave fluctuations yields a *subluminous* backscattered three-wave solitary structure, whose constant velocity is uniquely determined by the damping coefficients and the cw-pump level, and which is a universal attractor for any initial conditions in a compact support. This *Cauchy problem* of an initially bounded Stokes wave packet cannot yield a superluminous asymptotic traveling structure, since the front of the bounded wave packet propagates at the velocity of light.

(II) Initially *unbounded* Stokes conditions present well-known analytical *superluminous* [12] three-wave soliton solutions [13,14], also available for dissipative E_a and E_S envelopes [5,15,16]. Perturbative IST has been considered in the small dissipation case [17], but we shall see here (Sec. II) that the soliton solution is unstable in this case and is accompanied by a turbulent tail. Such turbulent behavior is reached via a bifurcation cascade from the stable dissipative one-soliton solution by decreasing the dissipation: it begins with a bisolitary structure, and is followed by a space-time-

*Electronic address: montes@unice.fr

dependent multipeak solitary regime for very small dissipation.

Besides this bifurcation scenario of the superluminous soliton solution, we present the stable family of asymmetric dissipative solitons for the general nonintegrable problem, resulting from the unlimited interaction at any dissipation (Sec. III). This family constitutes a continuous set of solitary attractors, backward traveling with respect to the continuous pump at velocities running from superluminous to subluminous, the dynamics dependent only on the wave-front slope p of the backscattered Stokes wave (slope-dependent velocity dispersion). An explicit solution for the integrable luminous velocity case is derived for the first time, to our knowledge. These stable solitary structures, generated by the backscattering three-wave instability, attain their nonlinear steady regime through dynamical compensation between the wave-front slope dispersion and the pump depletion (balance between *velocity dispersion steepening* and *nonlinear pump depletion flattening*), similarly to the well-known bright optical NLS (nonlinear Schrödinger) soliton [18], where compensation is achieved between the linear group-velocity dispersion and the nonlinear Kerr effect.

In Sec. IV, we shall determine a stability criterion for such structures by using an extension for this unbounded problem of the Kolmogorov, Petrovskii, and Piskunov (KPP) asymptotic procedure [19] used for the initially bounded case studied in paper I [10]. It will be shown that the subluminous attractor obtained in case (I) also belongs to the set of dissipative soliton solutions for unbounded conditions.

Finally, we present (a) experimental results in a cw-pumped Brillouin fiber-ring cavity showing trains of dissipative solitons at different velocities (having different slopes), (b) numerical simulation of the dynamics in such a cavity in order to point out the resemblance to the studied unlimited interaction, and (c) a classification scheme (summary) of the different dissipative three-wave solitary solutions.

Three-wave dissipative model

We deal with the space-time dynamics governed by the three-wave coherent model, relevant for instance in single-mode optical fibers [9,4]. The nonlinear resonant SBBS (or SRBS) process couples, through electrostriction (or through optically induced polarizability variations), a pump wave and a backscattered Stokes wave of complex amplitudes $E_p(\omega_p,k_p)$ and $E_S(\omega_S,k_S)$ to a material acoustic wave (or polarizability wave) $E_a(\omega_a=\omega_p-\omega_S,k_a=k_p+k_S)$. Neglecting the material wave propagation (since $c_a \ll c$ for SBBS), it yields, through the slowly varying envelope (SVE) approximation, the three coupled equations in dimensionless units [4],

$$
\begin{aligned}
(\partial_t+\partial_x+\mu_p)E_p&=-E_SE_a\,,\\
(\partial_t-\partial_x+\mu_S)E_S&=E_pE_a^*\,,\\
(\partial_t+\mu_a)E_a&=E_pE_S^*\,,
\end{aligned}
\tag{1}
$$

where the envelope amplitudes E_i, the time t, the space x variables, and the damping rates γ_i are normalized to the constant pump input E_{cw} and to the SBBS or SRBS coupling constant K [$E_i/E_{\rm cw}\to E_i$, $tKE_{\rm cw}\to t$, $xcKE_{\rm cw}/n\to x$, $\gamma_i(KE_{\rm cw})^{-1}\to\mu_i$ $(i=p,S,a)$].

Backward-traveling three-wave solutions

In order to obtain dissipative traveling three-wave structures, we must assume a constant pump input ($E_p=1$) compensating for the Stokes and material losses. Therefore, considering that the threshold condition is satisfied

$$
\mu_S\mu_a\equiv\frac{\gamma_S\gamma_a}{(KE_{\rm cw})^2}<1,
\tag{2}
$$

the E_S and E_a waves are unstable, exponentially growing in the linear parametric regime, until a nonlinear stage is reached, where the depletion of the pump E_p saturates the instability. The problem will be to determine the nonlinear three-wave solitary structures. In order to look for backward-traveling wave solutions of Eqs. (1), let us change to the frame moving in the backward direction $\zeta=x+Vt,\tau=t$,

$$
\begin{aligned}
[\partial_\tau+(1+V)\partial_\zeta]E_p&=-E_SE_a-\mu_pE_p\,,\\
[\partial_\tau+(V-1)\partial_\zeta]E_S&=E_pE_a^*-\mu_SE_S\,,\\
[\partial_\tau+V\partial_\zeta]E_a&=E_pE_S^*-\mu_aE_a\,.
\end{aligned}
\tag{3}
$$

Defining the A_i fields as

$$
A_p=|1+V|^{1/2}E_p\,,\quad A_S=|V-1|^{1/2}E_S\,,\quad A_a=|V|^{1/2}E_a\,,
\tag{4}
$$

and looking for stationary solutions in the new frame, which reduces the PDE problem to an ordinary differential equation (ODE) dynamical system, we have

$$
\begin{aligned}
\partial_XA_p&=-s_1A_SA_a-s_1\rho_pA_p\,,\\
\partial_XA_S&=s_2A_pA_a^*-s_2\rho_SA_S\,,\\
\partial_XA_a&=s_3A_pA_S^*-s_3\rho_aA_a\,,
\end{aligned}
\tag{5}
$$

where $X=\zeta/|(V-1)(1+V)V|^{1/2}$, $\rho_p=\mu_p|V-1|^{1/2}|V|^{1/2}/|1+V|^{1/2}$, and $\rho_S=\mu_S|1+V|^{1/2}|V|^{1/2}/|V-1|^{1/2}$, and $\rho_a=\mu_a|1+V|^{1/2}|V-1|^{1/2}/|V|^{1/2}$, and $s_1=\mathrm{sgn}(1+V)$, $s_2=\mathrm{sgn}(V-1)$, and $s_3=\mathrm{sgn}(V)$. Since $\mu_p\sim\mu_S\ll\mu_a$ and $V\sim1$ we also have $\rho_p\ll\rho_a$, but ρ_S and ρ_a are of the same order; then we can neglect the electromagnetic pump damping, which is necessary in order to define a local three-wave traveling solution [5]. Moreover, for the pure resonant problem, the relation between the three phases remains fixed and the whole dynamics is governed by real E_i or A_i fields, the negative amplitude standing for a π-phase shift.

II. DISSIPATIVE SYMMETRIC THREE-WAVE SOLUTION

First, let us recall the dissipationless case [13,14], which has been integrated by the inverse scattering transform [11]. The concept of self-induced transparency has been associated with this soliton solution [Fig. 1(a)], because all the pump is reconstructed after the interaction. This self-similar Stokes pulse travels at any superluminous velocity. In order to introduce the family of dissipative traveling wave struc-

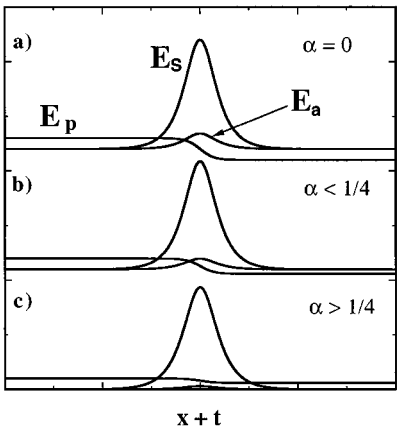

FIG. 1. Symmetric three-wave soliton solution: (a) Total self-induced transparency: nondissipative ($\alpha=0$) IST integrable soliton solution. (b) and (c) Partial self-induced transparency: dissipative soliton solution [Eqs. (10)]. (b) The pump wave exhibits a phase change ($\alpha<\frac{1}{4}$), and (c) the pump wave is weakly depleted without changing its phase ($\alpha>\frac{1}{4}$).

tures, our starting point will be the only known analytical superluminous soliton solution in the presence of dissipative Stokes ($\mu_S\neq 0$) and material ($\mu_a\neq 0$) waves [5]. This particular solution of system (5), is here called *symmetric*, since it is obtained for

$$\rho_S=\rho_a=\rho, \tag{6}$$

and is given by

$$A_p^0=-A\ \tanh AX+\rho, \quad A_S^0=A_a^0=A\ \mathrm{sech}AX, \tag{7}$$

where the limit conditions $[E_p(\zeta\rightarrow-\infty)=1$ and $E_{S,a}(\zeta\rightarrow-\infty)\rightarrow 0]$ determine the constant

$$A=(1+V)^{1/2}-\rho, \tag{8}$$

and fix the velocity $V=V_{\mathrm{sym}}$ as a function of (μ_a,μ_S),

$$V_{\mathrm{sym}}=\frac{1}{1-\mu_S/\mu_a}. \tag{9}$$

Let us write this *symmetric* solution of slope p_{sym} in the variables of Eq. (1):

$$\begin{aligned} E_p&=(\mu_S\mu_a)^{1/2}-[1-(\mu_S\mu_a)^{1/2}]\tanh[p_{\mathrm{sym}}(x+V_{\mathrm{sym}}t)],\\ E_S&=S\,\mathrm{sech}[p_{\mathrm{sym}}(x+V_{\mathrm{sym}}t)],\\ E_a&=S\left(\frac{\mu_S}{\mu_a}\right)^{1/2}\mathrm{sech}[p_{\mathrm{sym}}(x+V_{\mathrm{sym}}t)], \end{aligned} \tag{10}$$

where

$$\begin{aligned} S&=[1-(\mu_S\mu_a)^{1/2}][2(\mu_a/\mu_S)-1]^{1/2}p_{\mathrm{sym}},\\ &=\frac{[1-(\mu_S\mu_a)^{1/2}](1-\mu_S/\mu_a)}{(\mu_S/\mu_a)^{1/2}}. \end{aligned} \tag{11}$$

In the presence of weak dissipation ($\alpha\equiv\mu_S\mu_a<\frac{1}{4}$), the behavior is reminiscent of the self-induced transparency case: the pump wave being partially restored with an opposite phase after the interaction [Fig. 1(b)]. A property of this structure is then the possibility for the pump wave to change its phase, which is the key argument for the following stability discussion. When the Stokes and material waves are heavily damped $\alpha>\frac{1}{4}$, the pump is weakly depleted [Fig. 1(c)] without changing its phase.

Before describing the continuous family of three-wave dissipative solitary structures whose nonlinear dynamical behavior is obtained by the numerical treatment of Eqs. (1) for any dissipation and any initial wave-front slope conditions, let us look at the stability of the superluminous symmetric soliton solution.

Instability of the symmetric solution

Pitchfork bifurcation

We show here how this symmetric coherent structure decays through a cascade of bifurcations toward a turbulent tail structure for small dissipation, when the transmitted pump is strong enough to stimulate the Stokes and material waves again. We study the stability of solution (7) satisfying the ODE system (5) and being a particular traveling solution of the PDE (1), by looking what happens in its neighborhood. Defining

$$\rho_a=\rho+\epsilon/2,$$

$$\rho_S=\rho-\epsilon/2,$$

with $\epsilon\ll\rho$ and $2\rho=\rho_a+\rho_S$, we can linearize Eqs. (5) (with $s_i=1$ for $i=1$, 2, and 3 because $V_{\mathrm{sym}}>1$) around the analytical solution

$$A_i(X)=A_i^0(X)+\delta_i(X), \tag{12}$$

where $\delta_i\ll A_i^0$ and A_i^0 $(i=p,S,a)$ are given by Eq. (7). Introducing Eq. (12) into Eq. (5), defining $\delta=\delta_S-\delta_a$, and subtracting the last two equations of system (5), we obtain

$$\partial_X\delta=-\delta(A_p^0+\rho)+\epsilon A_S^0,$$

whose solution is

$$\delta(X)=\epsilon K(X)\exp(-2\rho X)\cosh(AX), \tag{13}$$

and where $K(X)$ is the following positive function:

$$K(X)=A\int_{-\infty}^{X}\exp(2\rho x)\,\mathrm{sech}^2(Ax)\,dx.$$

The two main points here are (i) δ has the same sign as ϵ, and (ii) for large X (but not too much in order to remain in the linear regime) there is an exponential dependence of δ with X,

$$\delta(X)\propto\exp(\lambda X), \tag{14}$$

where λ, obtained from expressions (6)–(8) with $\alpha=\mu_S\mu_a$, is given by

$$\lambda=1-\left(\frac{\alpha}{\alpha_c}\right)^{1/2}, \quad \alpha_c=\tfrac{1}{9}. \tag{15}$$

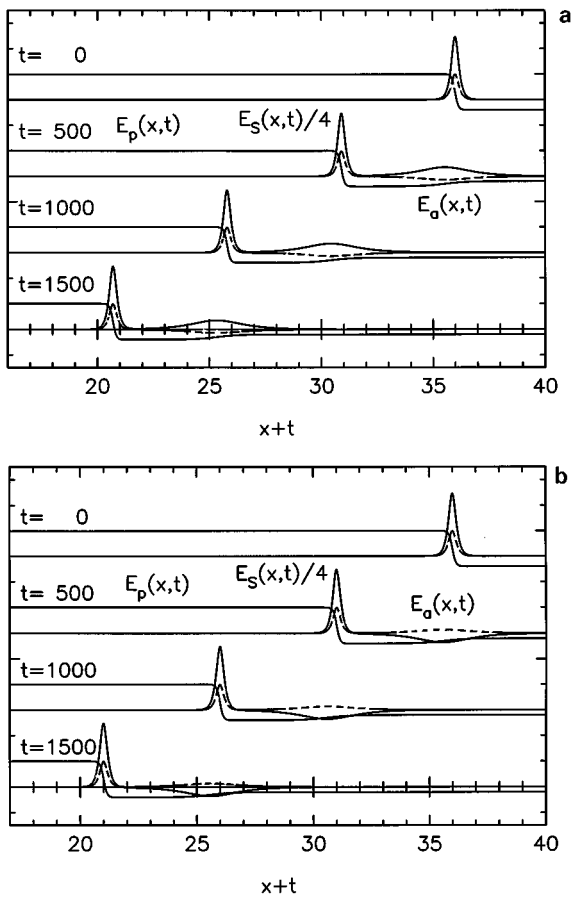

FIG. 2. Space-time evolution of the symmetric three-wave soliton solution for small dissipation ($\mu_a=3$, $\mu_S=3\times10^{-2}$, and $\alpha=9\times10^{-2}$) obtained by numerical computation of Eqs. (1) in the comoving Stokes frame $\xi=x+t$, giving rise to an asympotically stable bisolitary structure: (a) $\rho_a>\rho_S$, the material envelope exhibits a π phase change for the second peak; (b) $\rho_a<\rho_S$, the Stokes envelope exhibits a π phase change for the second peak.

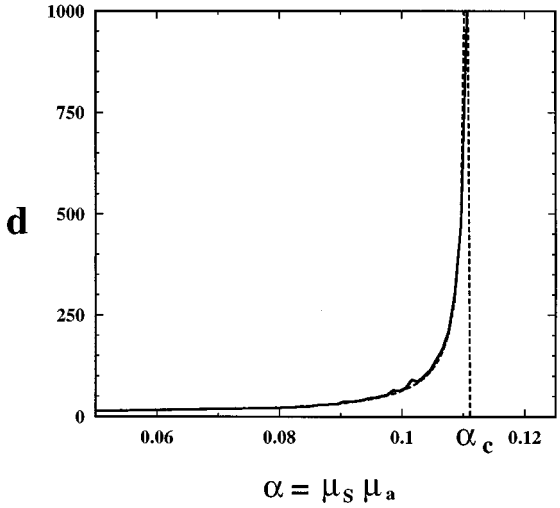

FIG. 3. Distance between the two pulses composing the bisolitary structure of Fig. 2 vs dissipation α resulting from the numerical dynamics (continuous curve) and from the analytical expression (16) (dashed curve).

For $\alpha>\alpha_c$, the perturbation is exponentially decreasing: the *symmetric* solution is stable. Otherwise, $\lambda>0$ for $\alpha<\alpha_c$, and the Stokes and material wave trajectories exponentially diverge at the rear part of the pulse. This result has a simple physical interpretation: the pump wave is reconstructed with an opposite phase ($\alpha<\frac{1}{4}$), and it is able to stimulate once again the Stokes and material waves.

We look at the nonlinear evolution of this instability until its saturation by numerically solving the spatiotemporal PDE Eqs. (1) in the comoving E_S frame ($\xi=x+t, \tau=t$), following the characteristics [20,9,10] and using a standard four order Runge-Kutta algorithm (see Appendix A). Starting from the unbounded *symmetric* solution, after a transient, two asymptotic stable traveling wave structures are reached [Figs. 2(a) and 2(b)] corresponding to the two possible ways of developing the instability depending on the sign of ϵ in Eq. (13). If $\epsilon>0$, then $\delta_S>\delta_a$, and the effective material wave damping ρ_a is greater than the Stokes one ρ_S ($\rho_a>\rho_S$), accounting for the phase change of the material amplitude [Fig. 2(a)]. The instability is saturated by exciting a second Stokes-material pulse. Otherwise, if $\rho_a<\rho_S$, the second pulse is also generated with opposite phases between the Stokes and material envelopes [Fig. 2(b)], but now operates a change of sign for the Stokes wave. The symmetry $A_S=A_a$ available for any $\alpha>\alpha_c$ is now broken. These properties are the characteristic features of a pitchfork bifurcation where the order parameter is $\delta=\delta_S-\delta_a$ and the control parameter is α. Therefore, for $\alpha<\alpha_c$, the *symmetric* solution is unstable and the nonlinear spatiotemporal dynamics reveals an interesting class of stable bisolitary solutions.

Distance between two pulses: critical behavior

A parameter which characterizes the bisolitary structure is the distance d between the two pulses and, as we can see in Figs. 2(a) and 2(b), it is conserved for every time. In fact, it characterizes the growth rate of the instability as is shown in expression (14). This distance is therefore proportional to λ^{-1},

$$d\propto\frac{1}{1-(\alpha/\alpha_c)^{1/2}}. \tag{16}$$

For $\alpha\lesssim\alpha_c$, the pump wave restored after the first pulse is just above threshold (2): the second pulse will be stimulated at infinity. This critical behavior of the ODE system is in excellent agreement with the numerical simulation of the nonlinear PDE system and we plot both determinations $d=d(\alpha)$ in Fig. 3.

Cascading towards turbulence

As the damping term α decreases, the pump wave—having generated the second Stokes-material pulse—may be sufficiently reconstructed (with two consecutive π-phase shifts) in order to stimulate again a third pulse, the process repeating for smaller values of α. Therefore, a set of peaks may be stimulated in cascade until exhausting the pump. A linear stability analysis, assuming the peaks to be independent of each other, yields the following formula for the critical value necessary to stimulate the $(n+1)$ multipeak structure:

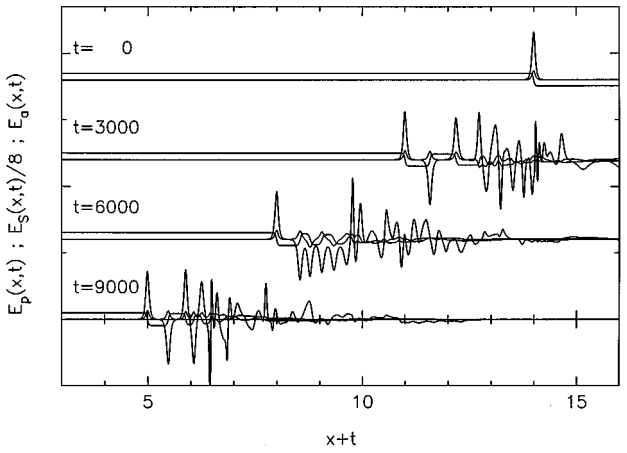

FIG. 4. Space-time evolution of the symmetric three-wave soliton solution for smaller dissipation than Fig. 2 ($\mu_a=1$, $\mu_S=10^{-3}$, and $\alpha=10^{-3}$), giving rise to a multipeak turbulent-tail structure. (The characteristic time t for SBBS is nanoseconds.)

$$\alpha_{c,n}=\frac{1}{(2n+1)^2}, \tag{17}$$

where $\alpha_{c,1}$ is the critical value of the pitchfork bifurcation. Therefore, just below $\alpha_{c,n}$, the $(n+1)$th pulse is excited at infinity and will rejoin the n-peak structure for $\alpha<\alpha_{c,n}$ following the critical behavior expressed in Eq. (16). A typical evolution of the *symmetric* solution for small enough α ($\mu_a=1$; $\mu_S=10^{-3}$) is plotted in Fig. 4. The Stokes envelope exhibits a set of large peaks, but no steady solitary behavior is reached. We can interpret this dynamics in the phase plane representation (where a two-dimensional projection is schematized in Fig. 5): the distortion and spreading of the trajectories are related to the homoclinic orbit corresponding to the analytical *symmetric* solution [Eq. (7)]. Starting from the unstable fixed point O (corresponding to $E_p=1$, and $E_S=E_a=0$), after achievement of the first loop it is not possible to predict the next ones. In fact, this sensitive zone related to the hyperbolic point O will split the trajectories towards either O' or O'', which are the two branches resulting from the pitchfork bifurcation. The E_i fields becoming turbulent, we cannot predict how many peaks will be positive or negative in the Stokes or material spatiotemporal evolution until the dissipation ends to contract the rear part of the structure (Fig. 4).

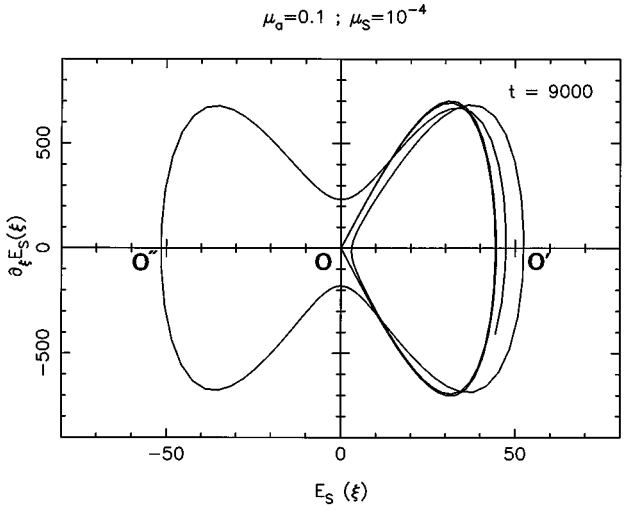

FIG. 5. Phase plane representation (Stokes amplitude and its derivative) vs parameter $\xi=x+t$, showing the sensitive zone around the hyperbolic point O. Starting from the unstable fixed point O, the plot of the trajectories is stopped after few right loops (toward O') and one left loop (toward O''), the two branches of a pitchfork bifurcation.

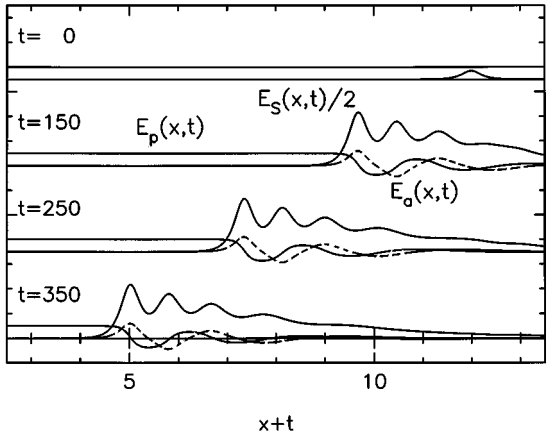

FIG. 6. Space-time evolution of an initial Stokes condition having a slope $p=0.9p_{\rm sym}=7.45$ with dissipation ($\mu_a=1$, $\mu_S=10^{-2}$, and $\alpha=10^{-2}$) yielding a traveling multipeak three-wave structure.

We may point out in Fig. 4 that *symmetric* solutions seem to escape from the turbulent tail of the structure. This behavior is very evident as we approach the nondissipative integrable problem ($\alpha=0$) where superluminous solitons leave from the radiative envelope (π-pulse-type structure) propagating at the light velocity [21], the word ''radiation'' here being opposed to ''soliton.'' Therefore, *weak dissipation traps the radiation leading to turbulent-tail solitary structures.*

III. ASYMMETRIC THREE-WAVE DISSIPATIVE SOLITONS

In Sec. II, we explored the spatiotemporal behavior for any damping value α, still remaining in the vicinity of the *symmetric* solution [Eqs. (7) and (10)], which satisfies Eq. (6), characterized by its wave-front slope $p_{\rm sym}$ (11) and its velocity $V_{\rm sym}$ (9). This solution being the only localized backward-traveling three-wave structure in the dissipationless case [13,14], our aim here is to show how the damping reveals a family of asymmetric solitary structures when condition (6) is no longer verified. Moreover, even for small damping values ($\alpha\ll\alpha_c$, $p\neq p_{\rm sym}$), the Stokes and material trajectories in the phase plane representation swerve from the sensitive homoclinic orbit (Fig. 5), which caused turbulence, and a steady solitary attractor is once again reached. As an example, in Fig. 6 we plot the numerical space-time evolution for an initial Stokes condition having a wave-front slope $p=0.9p_{\rm sym}$ ($\alpha=10^{-2}<\alpha_c$), yielding a steady multipeak structure. This modulated profile is progressively smoothed as the initial wave-front slope p deviates from the symmetrical value $p_{\rm sym}$. Typical shapes of solitary structures, for dif-

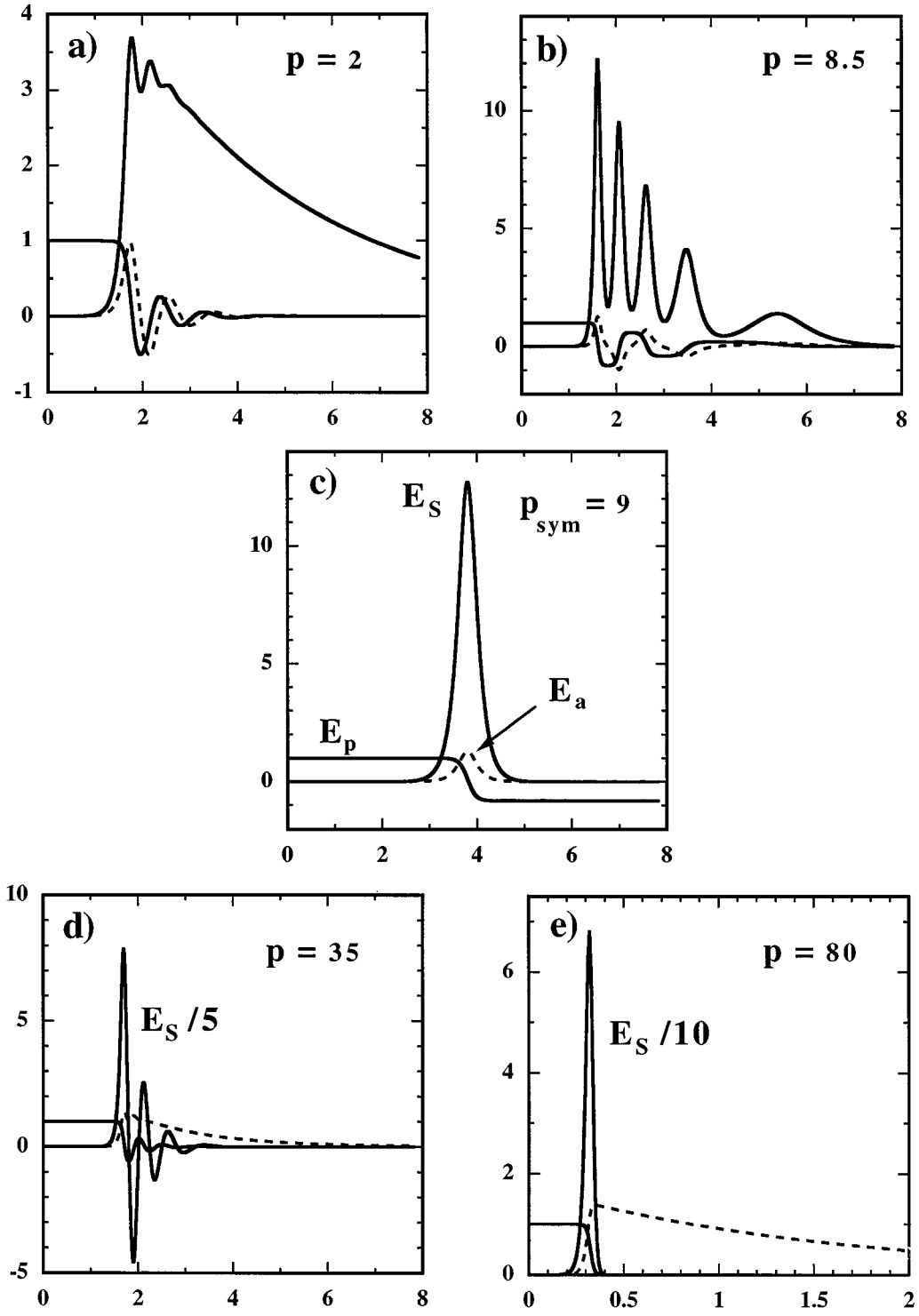

FIG. 7. Asymptotic dissipative ($\mu_a=1$, $\mu_S=10^{-2}$, $\alpha=10^{-2}$) three-wave structures for the following. $\rho_S<\rho_a$ and $p<p_{\rm sym}$: (a) $p=2$, (b) $p=8.5$, and (c) $\rho_S=\rho_a$ and $p=p_{\rm sym}=8.91$. $\rho_S>\rho_a$ and $p>p_{\rm sym}$: (d) $p=35$ and (e) $p=80$.

ferent wave-front slopes p, and a fixed damping value $\alpha=10^{-2}<\alpha_c$, are plotted in Fig. 7. All these solitary structures prove numerically stable in the asymptotic regime, like that shown in Fig. 6. For $\rho_S<\rho_a$ [Fig. 7(a) and 7(b)], we note how broad and flat the Stokes envelope is compared to the *symmetric* solution [Fig. 7(c)]. The resulting slope p, is smaller and the corresponding velocity V will be greater, as we shall see in Sec. IV. On the other hand, for $\rho_a<\rho_S$, we obtain a narrowed pulse [Fig. 7(d) and 7(e)] with a corresponding smaller velocity. In fact, the velocity can even be subluminous.

In order to summarize the complex spatiotemporal dynamics, the domain of stability is schematized in the (p,α) plane [Figs. 8(a) and 8(b)]. Figure 8(a) roughly shows the domain of stable one-peak dissipative solitary structures ($\alpha_c<\alpha<1$) and the domain of multipeak turbulent-tail

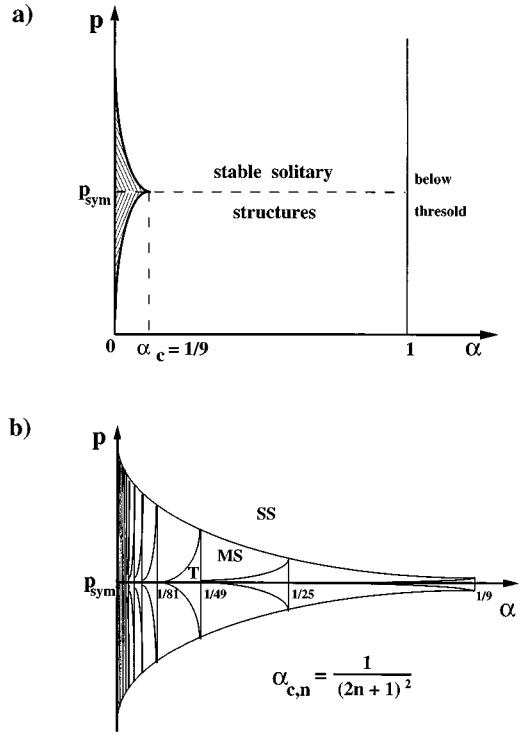

FIG. 8. Stability domain in the (p,α) plane: (a) Whole instability domain ($\alpha<1$), where stable dissipative asymmetric structures are formed, (b) magnification of the region of small dissipation ($\alpha<\alpha_c=\frac{1}{9}$) where single-peak solitary (SS), multipeak solitary (MS), and multipeak turbulent structures (T) are formed, depending on the nearness with respect to the symmetrical wave-front slope $p_{\rm sym}$.

structures (shaded region: $0<\alpha<\alpha_c$). Figure 8(b) is a magnification of the last region showing the stable one-peak solitary structure domain, and the multipeak structure domain itself containing the time-dependent cascading areas (T), where the multipeak structures are accompanied by turbulent tails. These areas become thinner and closer together, according to Eq. (17), as the damping α decreases, until they constitute a foliated zone in the vicinity of $\alpha=0$, to which is associated a turbulent tail.

Luminous backward-traveling three-wave solution

For the particular case of the three-wave backward-traveling solution at the velocity of light ($V=1$), the nonintegrable three-wave PDE equation system (3) reduces to the problem of two ODE equations which we are able to integrate. Indeed, the second equation (3) yields

$$E_S=\frac{E_pE_a^*}{\mu_S}, \tag{18}$$

and we obtain a two-equation system for the pump and material wave intensities ($I_{p,a}=|E_{p,a}|^2$), where the Stokes wave plays the role of a slave variable,

$$\frac{dI_p}{dX}=-I_pI_a, \tag{19a}$$

$$\frac{dI_a}{dX}=2I_pI_a-2\alpha I_a, \tag{19b}$$

with $X=\zeta/\mu_S$ and $\alpha=\mu_S\mu_a$. Introducing the change

$$I_p=\exp(W-1/\alpha), \tag{20}$$

Eq. (19a) verifies

$$I_a=-\frac{dW}{dX}, \tag{21}$$

and the equations system (19a) and (19b) is reduced (see Appendix B) to the integral

$$\frac{dW}{d\eta}=\exp W-aW, \tag{22}$$

where $\eta=2X\exp(-1/\alpha)\}$, and the constant $a=\alpha\exp(1/\alpha)$ is determined by the limit condition $I_p(X\to-\infty)=1$. Equation (22) is of the separation of variables form, but no analytical solution is available. It may be easily integrated by a numerical Runge-Kutta algorithm. For $a>\mathbf{e}$, (i.e., for the localization threshold condition $\alpha=\mu_S\mu_a<1$), we obtain two finite values of W, say W_1 and W_2, solutions of

$$\exp W-aW=0 \Rightarrow (W_1,W_2) \quad \text{for } a>e,$$

where all the derivatives of W vanish for $\eta\to\pm\infty$. For $I_p(X\to-\infty)=1$ we have $W_2=1/\alpha$. Knowing $W=W(\eta)$, Eq. (20) yields a traveling localized structure of the kink form for I_p, and from Eq. (21) of the asymmetric pulse form for I_a and I_S,

$$I_a=-\frac{dW}{d\eta}\frac{d\eta}{dX}=-2\exp(-1/\alpha)(\exp W-aW), \tag{23}$$

$$I_S=\frac{I_pI_a}{\mu_S^2}, \tag{24}$$

which are represented in Fig. 9(a). The maximum of I_a, obtained from $dI_a/dX=0$, at $W_{a,\max}=a$, is given by

$$I_{a,\max}=2\alpha(\ln\alpha+1/\alpha-1), \tag{25}$$

and the maximum of the Stokes pulse I_S [obtained from $dI_S/dX=0$, at $W_{S,\max}$, solution of $\exp W_{S,\max}=(1+a)W_{S,\max}/2$], is given by

$$I_{S,\max}=\frac{1}{2\mu_S^2}[\alpha^2-\exp(-2/\alpha)]W_{S,\max}^2. \tag{26}$$

For example, let us take $\alpha=\mu_S\mu_a=0.625$; then we have $a=\alpha\exp(1/\alpha)=3.095\,64$, $W_2=1/\alpha=1.6$, $W_1=0.5724$, and $I_p(\zeta\to+\infty)=\exp(W_1-W_2)=0.3578$, which are in perfect agreement with the space-time numerical simulation of Eqs. (3), namely, $E_p(\zeta\to\infty)=\sqrt{I_p(\zeta\to+\infty)}=0.5983$.

Even if this luminous solution is a particular one, it turns out to be one of the most interesting attractors, since we can approach it in an actual Brillouin fiber-ring experiment, as we shall see in Sec. V. In Fig. 9(b) we show the three-amplitude luminous structure for $\alpha=9\times10^{-2}$ ($\mu_a=3$; $\mu_S=3\times10^{-2}$), associated with an actual experiment.

IV. STABILITY CRITERION: ASYMPTOTIC PROCEDURE

In Sec. III we showed the existence of a family of asymptotically stable three-wave dissipative solitary structures whose velocity can be superluminous or subluminous de-

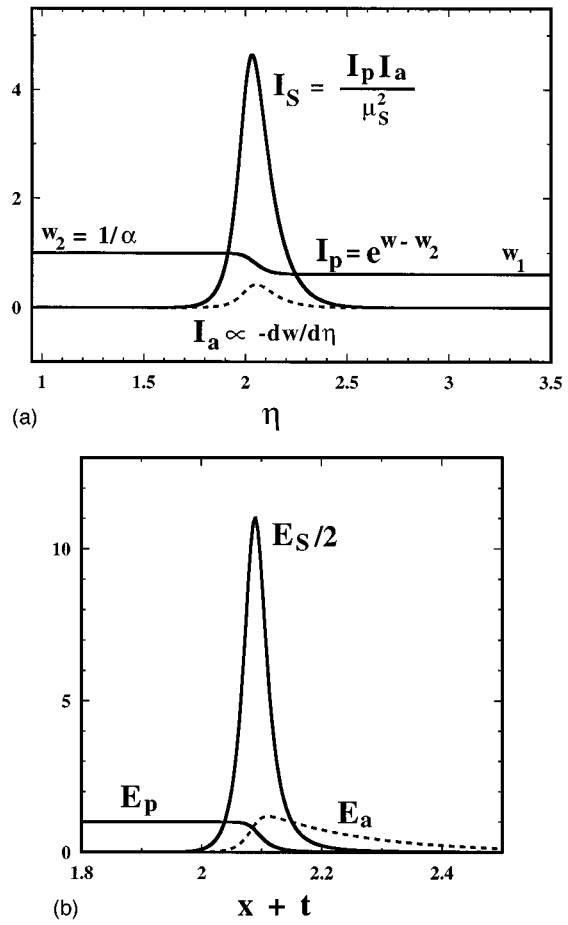

FIG. 9. Luminous three-wave backward-traveling solution: (a) Shape of the analytical solutions (20), (23), and (24) for $\alpha=0.625$. (b) Asymptotic three-wave (luminous) amplitude structure for $\mu_a=3$ and $\mu_S=3\times10^{-2}$ ($\alpha=9\times10^{-2}$) resulting from the space-time dynamical evolution.

pending on the wave front slope p of the backscattered or material wave. An explicit solution for the particular integrable luminous velocity case has also been given. The object here is to determine the stability criterion for all these structures by using an extension of the (already used [10]) KPP asymptotic procedure [19] for this unbounded problem, in order to find the long term evolution of initially unbounded Stokes or material envelopes in the presence of a cw pump. The main property found is the existence of a particular solution (coinciding with the subluminous attractor of paper I), corresponding to the minimum authorized velocity V_0, which turns out to be the frontier of stability for the entire family of backward-traveling wave structures. For details the reader can see Appendix C.

Considering that the threshold condition (2) is satisfied ($\mu_S\mu_a<1$), the Stokes and material waves are unstable, and exponentially growing in the linear parametric regime. The instability is then saturated by the pump depletion and the three envelopes self-structure into a solitary wave. For an initially unbounded Stokes or material condition, the asymptotic procedure analytically determines the velocity and the slope of the wave front in the linear regime of the undepleted pump, which turns out to be the value of the velocity in the nonlinear steady state of strong pump depletion, since the front edge of the whole three-wave steady structure remains in the linear undepleted pump regime every time.

Thus, assuming an undepleted pump wave ($E_p=1$) throughout the whole linear interaction range, from Eqs. (1) we obtain the linearized equation set

$$(\partial_t-\partial_x+\mu_S)(\partial_t+\mu_a)E_{S,a}=E_{S,a}\,, \tag{27}$$

whose characteristic equation for an exponential dependence [$E_{S,a}\propto \exp(\gamma t+px)$] reads

$$(\gamma-p+\mu_S)(\gamma+\mu_a)=1, \tag{28}$$

where we only keep the unstable root ($\mathrm{Re}\,\gamma>0$)

$$\gamma=\frac{p-\mu_a-\mu_S}{2}+\frac{\sqrt{(p+\mu_a-\mu_S)^2+4}}{2}. \tag{29}$$

The solution of this linear problem may be given by means of the Fourier transform (with $p=-ik$ and k complex):

$$E_{S,a}(x,t)=\int_{-\infty}^{\infty}\widetilde{E}_{S,a}(p)\exp(\gamma(p)t)\exp(px)dp$$

where $\widetilde{E}_{S,a}(p)$ is the Fourier transform of the initial condition $E_{S,a}(x,t=0)$. Let us look for backward-traveling waves with velocity V,

$$\zeta=x+Vt,$$

yielding

$$E_{S,a}(\zeta,t)=\int_C \widetilde{E}_{S,a}(p)\exp[\gamma(p)-pV]t\,\exp(p\zeta)dp. \tag{30}$$

This linear solution holds for long times t, allowing us to obtain the asymptotic behavior of the far pulse wave front, where the linear undepleted pump approximation always remains valid. As a result of the parametric instability, the asymptotic wave front structure grows exponentially. Since we are interested here in characterizing the whole family of backward-traveling wave structures, we will only consider the exponential head-front dependence; then the corresponding Fourier transform $\widetilde{E}_{S,a}(p)$ has a pole. Moreover, the function $f(p)=\gamma(p)-pV$ has a saddle point, and the integral can then be performed by the steepest descent method. Therefore, it may be shown (see Appendix C), that the pole asymptotically dominates over the saddle point for any slope p smaller than a critical value p_0 ($p<p_0$). The stationarity of the three-wave structure in its backward-traveling frame then imposes

$$V(p)=\frac{\gamma(p)}{p}=\frac{1}{2}-\frac{\mu_S+\mu_a}{2p}+\frac{\sqrt{(\mu_a-\mu_S+p)^2+4}}{2p} \tag{31}$$

where the *amplitude velocity* of the traveling wave structure is then defined as the quotient between the temporal (γ) and spatial (p) growth rates. We plot this velocity dispersion relation (31) in Fig. 10.

In the opposite case $p>p_0$, it is the saddle point which dominates the long-term behavior, and, following the steepest descent method [22], the supplementary condition is

$$V=[\partial\gamma(p)/\partial p]_{p=p_0}. \tag{32}$$

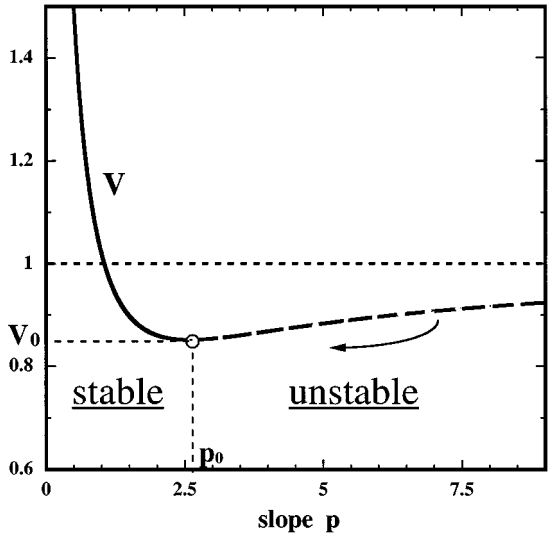

FIG. 10. Velocity dispersion: Amplitude velocity $V=\gamma/p$ of the dissipative three-wave structure vs the exponential slope p of the backscattered wave front showing the stable ($p<p_{\mathrm{sym}}$) and unstable ($p>p_{\mathrm{sym}}$) domains.

The velocity and the head-front slope then become fixed by Eqs. (31) and (32),

$$V_0=\frac{2+\mu_a^2-\mu_S\mu_a+2\sqrt{1-\mu_S\mu_a}}{4+(\mu_a-\mu_S)^2}, \tag{33}$$

$$p_0=\frac{1}{\mu_S}+\mu_S-\frac{1}{\mu_a}-\mu_a+\frac{\sqrt{1-\mu_S\mu_a}}{\mu_a}+\frac{\sqrt{1-\mu_S\mu_a}}{\mu_S}. \tag{34}$$

Hence this particular solution, which stands at the bottom of the $V(p)$ curve of Fig. 10, separates the stable ($p<p_0$) and the unstable domains ($p>p_0$). Moreover, such a solution is an attractor for any initial condition having a wavefront slope $p>p_0$.

Let us finally point out the strength of this method, which allows us to determine the nonlinear stage of the interaction by simply looking at the linear asymptotic evolution of its wave front, and characterizes the continuous family of three-wave solitary attractors analyzed in Secs. II and III. In order to test this statement with an additional example, we considered an initial Gaussian condition for the Stokes envelope. The slope of its frontal tail being greater than any exponential one, it is expected from this theory that only the saddle point contributes to integral (30); the numerical evolution confirms this behavior and the corresponding fundamental subluminous attractor is asymptotically reached (Fig. 11).

The reader may now ask: How could an initially bounded condition (paper I) yield the same asymptotic solution as that obtained for a particular subluminous case of an initially unbounded condition? This can be possible due to the subluminous velocity of the structure formed from the initially bounded condition, since it becomes asymptotically decorrelated from its luminous tip of the foot at the beginning of the interaction.

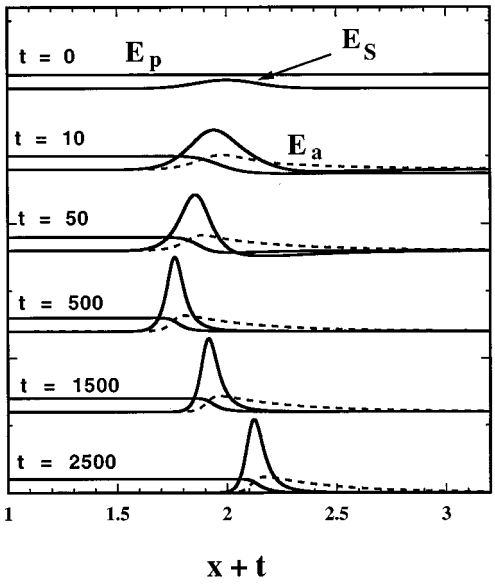

FIG. 11. Space-time evolution of an initial Gaussian Stokes condition. The wave-front tail profile being steeper than any exponential slope, the solitary structure is attracted by the subluminous (p_0,V_0) solution.

Balance between velocity dispersion and pump depletion

In fact, this stability problem has a fundamental physical significance. Let us remark upon its resemblance to the well-known bright optical NLS soliton [18], where compensation between the linear dispersion and the nonlinear Kerr effect is only possible for negative dispersion of the group velocity ($\partial\omega/\partial k$). Here, for the three-wave soliton, the *amplitude velocity* γ/p stands for the group velocity, the linear effect is the backscattering instability characterized by its growth rate p, and the nonlinear effect is the pump depletion. Figure 10 shows that the velocity dispersion now depends on the slope (instead on the wave number for the NLS soliton). In our case, if the velocity dispersion ($\partial V/\partial p<0$) allows the smaller slopes to rejoin the higher ones (since their velocity is greater), a balance may be achieved between *velocity dispersion steepening* and *nonlinear pump depletion flattening*. This case corresponds to stable soliton solutions ($p<p_0$). Otherwise ($p>p_0;\partial V/\partial p>0$), both effects act in the same way and tend to flatten the three-wave structure, which spreads until reaching the subluminous attractor (p_0,V_0), given by Eqs. (33) and (34), and described in paper I.

V. BRILLOUIN FIBER-RING LASER PULSES

The present theoretical study of an unlimited interaction is useful to enlight the nonlinear dynamics in a cw-pumped Brillouin fiber-ring laser, where solitonic pulses are obtained below a critical feedback R_{crit} and interpreted via a Hopf bifurcation process from the steady Brillouin mirror solution [6].

We performed long-time numerical simulations of Eqs. (1) for a ring configuration of length L corresponding to the experiment of Ref. [6], with periodic boundary conditions for the Stokes wave,

$$E_p(x=0,t)=E_{cw}=\mathrm{const}, \quad E_S(x=L,t)=\sqrt{R}E_S(x=0,t) \tag{35}$$

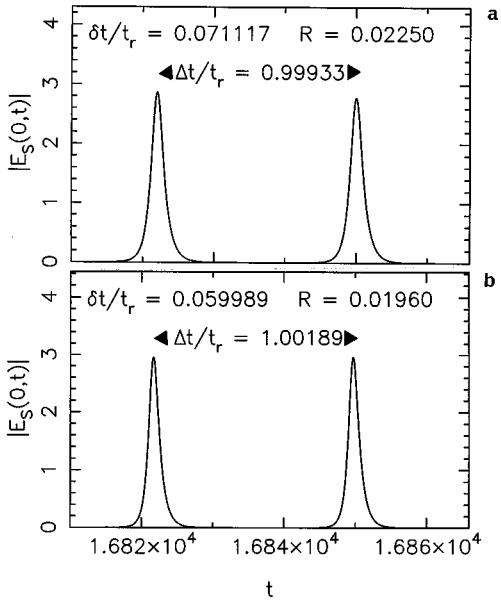

FIG. 12. Backscattered asymptotic pulses at the output of the Brillouin fiber-ring cavity of Ref. [6], obtained from numerical integration of Eqs. (1) with boundary conditions (35) for a SBBS gain length $G=gLI_{cw}=8$. (a) Superluminous regime ($\Delta t/t_r=0.99933$, $V>1$) corresponding to a Stokes intensity feedback $R=0.0225$. (b) Subluminous regime ($\Delta t/t_r=1.00189$, $V<1$) for $R=0.0196$.

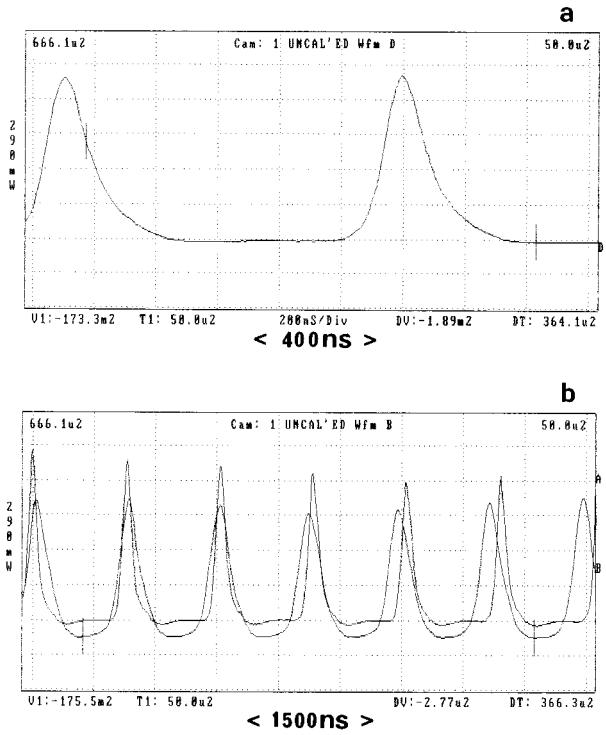

FIG. 13. Experimental recording of different trains of solitary Stokes pulses at the output of the 250-m fiber-ring cavity (whose characteristics are given in Table I) corresponding to a feedback near $R_{\rm crit}$ and a gain length of about $G=4$. (a) The shape presents a great resemblance to the asymmetric luminous dissipative soliton shown in Fig. 9(b). (b) Comparison of two superimposed trains of pulses in order to show that the lower slopes correspond to the faster train, as predicted by the theory.

in the solitonic feedback range ($R_{\rm thres}<R<R_{\rm crit}$), and in Fig. 12 we plot the backscattered asymptotic pulses at the output of the ring cavity. Each pulse corresponds to one round trip, and the distance between them measures the mean round-trip period Δt normalized to the photon round-trip time $t_r=nL/c$. We can see that both slightly superluminous ($\Delta t/t_r<1$) and subluminous ($\Delta t/t_r>1$) regimes are available for the same configuration, by varying the feedback control parameter R for the same gain length $G=gLI_p=8$.

Moreover, the width δt of the pulses, which is inversely proportional to the exponential slope p, is narrower for smaller velocities in agreement with the dispersion curve of Fig. 10.

TABLE I. Computation parameters for the Nd-YAG (yttrium aluminum garnet) cw-pumped Brillouin fiber ring laser. The active medium is a single-mode optical-fiber of length $L=250$ m, with a 11.3-μm-diameter Ge-doped core ($n_0=1.44$), and effective optical cross section $S=10^{-10}$ m^2. The pump wavelength is $\lambda=1.319$ μm (acoustic wavelength $\lambda_a=0.43$ μm). The coherent SBS coupling constant entering the normalization of Eqs. (1) is given by $K=(1/\sigma)[(\varepsilon_0 c n_0^7)/(2\rho_0 c_a)]^{1/2}(\pi p_{12}/\lambda)=17.8$ m s^{-1} V^{-1}, where $\sigma\simeq\sqrt{2}$ is the depolarization factor. P is the pump power coupled into the fiber, $I_p=P/S$ is the pump flux intensity, $G=gLI_p$ is the dimensionless SBS intensity gain length [$g=4K^2/(\gamma_a\varepsilon_0 c^2)$], E_p is the pump amplitude corresponding to $I_p=(n_0\varepsilon_0 c/2)|E_p|^2$, $\tau=(KE_p)^{-1}$ is the coherent SBS characteristic time, $\mu_a=\gamma_a\tau$ is the dimensionless acoustic damping rate ($\gamma_a=\pi\Delta\nu\simeq 6.94\times 10^7$ s^{-1}), $\mu_e=\gamma_e\tau$ is the dimensionless optical damping rate ($\gamma_e\simeq 9.35\times 10^3$ s^{-1}, spatial intensity attenuation $2n_0\gamma_e/c=0.39$ dB km^{-1}), $R_{\rm crit}=1/[3\exp(G/3)-2]$ is the critical Stokes intensity feedback for pulse formation [6], and $R_{\rm thres}=\exp(-G)$ is the laser threshold feedback.

P[mW]	34.7	69.5	104.2	139	173
I_p[MW/cm^2]	0.0347	0.0695	0.104	0.139	0.173
$G=gLI_p$	2	4	6	8	10
E_p(MV/m)	0.427	0.604	0.739	0.855	0.954
$\tau=(KE_p)^{-1}$(ns)	131	93.0	76.0	65.6	58.5
$\mu_a=\gamma_a\tau$	9.09	6.45	5.27	4.55	4.06
$\mu_e=\gamma_e\tau$	1.2×10^{-3}	8.7×10^{-4}	7.1×10^{-4}	6.1×10^{-4}	5.4×10^{-4}
$R_{\rm crit}$	0.26	0.106	0.049	0.024	0.012
$R_{\rm thres}$	0.13	0.018	0.0024	3.3×10^{-4}	4.5×10^{-5}

Experimental results

In order to test the universality of our results, we performed additional experiments in another cw-pumped Brillouin fiber-ring cavity, the experimental setup being the same as in [6], and the characteristics given in Table I. In Figs. 13(a) and 13(b) we plot the experimental recording of different trains of solitary Stokes pulses at the output of the 250-m fiber-ring cavity. Figure 13(a) shows a pair of solitary pulses for a feedback just below R_{crit}, and a gain length of $G=4$ ($P\simeq 70$ mW) corresponding to values of column 2. Their shape has a great resemblance to the asymmetric luminous dissipative soliton shown in Fig. 9(b). We can measure a time width $\delta t=0.153\pm 0.004$ μs, which is inversely proportional to the exponential slope p, and a mean round-trip period of $\Delta t=1.087\pm 0.004$ μs, which is inversely proportional to the velocity. In order to compare better the different round-trip periods for different slopes, controlled in the experiment by varying the feedback between R_{crit} and R_{thres}, in Fig. 13(b) we show two superimposed trains of solitons. We remark that the lower slopes correspond to the faster train. Subsequent study must be done in order to understand the whole nonlinear dynamics in a lossy fiber-ring cavity, but the present results are highly encouraging.

VI. SUMMARY: PARAMETER'S CLASSIFICATION SCHEME

α	p	V	ρ_a	ρ_S	Dissipative three-wave soliton solutions
0	>0	>1	0	0	IST integrable total self-induced transparency: 3-W soliton solution
0	>0	>1	>0	0	integrable full pump-Stokes conversion (damped pendulum)
>0	>0	1			integrable particular luminous solution (one peak)
$\ll\alpha_c=\frac{1}{9}$	p_{sym}	V_{sym}	ρ_S	ρ_a	integrable unstable solution
	$\simeq p_{\mathrm{sym}}$	$\simeq V_{\mathrm{sym}}$	$\simeq\rho_S$	$\simeq\rho_a$	nonintegrable chaotic structure
$<\alpha_c$	$<p_{\mathrm{sym}}$	$\simeq V_{\mathrm{sym}}$	$\simeq\rho_S$	$\simeq\rho_a$	nonintegrable attractor, multipeak traveling structure (in phase)
	$>p_{\mathrm{sym}}$	$\simeq V_{\mathrm{sym}}$	$\simeq\rho_S$	$\simeq\rho_a$	*ibid.* (alternate phases)
	$<p_0$	$> V_0$	$\neq\rho_S$	$\neq\rho_a$	nonintegrable attractors from multi-peak to one peak struct.
	$>p_0$	$\rightarrow V_0$	$\ll\rho_S$	$\gg\rho_a$	non-integrable unstable evolving to $(p_0,\ V_0)$ attractor
$\alpha_c=\frac{1}{9}$	$\cong p_{sym}$	$\cong V_{sym}$	$\cong\rho_S$	$\cong\rho_a$	pitchfork bifurcation (cf. section 2.1)
$>\alpha_c=\frac{1}{9}$	p_{sym}	V_{sym}	ρ_S	ρ_a	integrable stable one peak attractor
	$<p_0$	$>V_0$	$\neq\rho_S$	$\neq\rho_a$	non-integrable attractor one peak
	$>p_0$	$\rightarrow V_0$	$\ll\rho_S$	$\gg\rho_a$	non-integrable unstable evolving to $(p_0,\ V_0)$ attractor

VII. CONCLUSION

We found a continuous set of asymptotically stable superluminous and subluminous dissipative three-wave solitary attractors for the initially unbounded Stokes problem in the presence of a continuous pump wave, dependent only on the wave-front exponential slope p of the backscattered Stokes envelope. These dissipative three-wave solitons result from the dynamical compensation between negative velocity dispersion ($\partial V/\partial p<0$) and pump depletion, their stability being justified by an extension of the Kolmogorov, Petrovskii, and Piskunov asymptotic procedure to this unbounded problem. This dissipative soliton family completes the known superluminous symmetric soliton solution and is in agreement with optical Brillouin fiber-ring laser experiments. Moreover, the symmetric soliton solution, is proved to be unstable for small dissipation exhibiting a turbulent multipeak tail, *via* a cascading process from the stable bisolitary structure, with the dissipation (damping) as the control pa-

rameter. This turbulence limits the analytical perturbative approach [17] obtained for $\alpha \ll 1$ to a description for the short time evolution.

ACKNOWLEDGMENTS

The authors thank J. Botineau, J. Coste, D. J. Kaup, O. Legrand, A. Mikhailov, and E. Picholle for their valuable comments and help in this work.

APPENDIX A

Let us consider the nonlinear space-time evolution of the three-wave system governed by Eqs. (1) for an initially unbounded Stokes condition $E_S(x,t=0)$ exponentially decreasing at $x \to -\infty$, and counterpropagating with respect to the continuous pump $E_p(x,t=0)$. Since we are looking for solutions localized in the vicinity of the E_S characteristic, it is natural to reduce the problem to the initial-boundary value problem in the comoving E_S frame ($\xi = x+t, \tau = t$), where Eqs. (1) read

$$\begin{aligned} (\partial_\tau + 2\partial_\xi) E_p &= -E_S E_a, \\ (\partial_\tau + \mu_S) E_S &= E_p E_a^*, \\ (\partial_\tau + \partial_\xi + \mu_a) E_a &= E_p E_S^*, \end{aligned} \tag{A1}$$

with the initial condition $E_S(\xi \propto \mathrm{sech}(p\xi), \tau = 0)$, and supplemented boundary conditions at $\xi = 0$, $E_p(\xi = 0, \tau) = 1$ and

$$E_a(\xi=0,\tau) = [E_S(\xi=0,\tau)/2][-p-\mu_a+\mu_S + \sqrt{4+(\mu_a-\mu_S+p)^2}].$$

It is convenient, for numerical integration, to remove the space derivatives from Eqs. (A1) by introducing other functions $Z_i(\xi,\tau)$ defined by

$$\begin{aligned} Z_p(\xi,\tau) &= E_p(\xi+2\tau,\tau), \\ Z_S(\xi,\tau) &= E_S(\xi,\tau), \\ Z_a(\xi,\tau) &= E_a(\xi+\tau,\tau). \end{aligned} \tag{A2}$$

Then the Z_i's obey the following nonlocal equations in ξ:

$$\begin{aligned} \partial_\tau Z_p(\xi,\tau) &= -Z_S(\xi+2\tau,\tau) Z_a(\xi+\tau,\tau), \\ (\partial_\tau + \mu_S) Z_S(\xi,\tau) &= Z_p(\xi-2\tau,\tau) Z_a(\xi-\tau,\tau), \\ (\partial_\tau + \mu_a) Z_a(\xi,\tau) &= Z_p(\xi-\tau,\tau) Z_S(\xi+\tau,\tau). \end{aligned} \tag{A3}$$

Discretizing the ξ variable (through $\xi_j = j\not{\delta}$), we obtain a set of functions Z_α^j obeying ordinary differential equations. These equations will be considered to depend explicitly on time through the spatial arguments of the Z_α^j functions, namely, $\xi \pm \tau$, $\xi \pm 2\tau$. We can then apply a standard Runge-Kuttta algorithm to the numerical integration of these equations. However, we must consider the stability of this algorithm. It is known, in the case of PDE describing counterstreaming wave interaction that a numerical instability occurs when the spatial step $\not{\delta}$ is larger or equal to the temporal step $\not{\delta}_0$. We have therefore been led to use $\not{\delta} = \not{\delta}_0/2$. Then at each step of integration the pairwise values Z_α^j are incremented according to the Runge-Kutta algorithm, while the odd ones are calculated by four-term interpolation using the pairwise values Z_α^j. This procedure proves to be remarkably stable.

APPENDIX B

From Eq. (19a) we have $I_a = -I_p'/I_p$, where the prime stands for the derivative with respect to X. Differentiating once more and eliminating I_a' from Eq. (19b), we obtain a closed second order differential equation for I_p,

$$\frac{d}{dX}\left[\left(\frac{I_p'}{I_p}\right) - 2I_p + 2\alpha \ln I_p\right] = 0. \tag{B1}$$

Introducing the change $I_p = \exp U$, which satisfies $dU/dX = I_p'/I_p = -I_a$, Eq. (B1) is reduced to a first order differential equation

$$\frac{dU}{dX} = 2\,\exp U - 2\alpha U + C,$$

where C is a constant that can be removed with the change $\{[W = U - C/(2\alpha);\ \eta = 2X\,\exp[C/(2\alpha)]\}$, yielding

$$\frac{dW}{d\eta} = \exp W - aW, \tag{B2}$$

and where the constant $a = \alpha\,\exp[-C/(2\alpha)] = \alpha\,\exp(1/\alpha)$ is determined from the limit condition $I_p(X \to -\infty) = 1$. Equation (B2) is of the separation of variables form, but no analytical solution is available. It may be easily integrated by a numerical Runge-Kutta algorithm.

APPENDIX C

The basic equations (1) linearized in the parametric ($E_p = 1$) regime are

$$(\partial_t - \partial_x + \mu_S)(\partial_t + \mu_a) E_{S,a} = E_{S,a},$$

whose characteristic equation $\gamma(k)$ for an exponential dependence [$E_{S,a} \propto \exp(\gamma t - ikx)$] reads

$$(\gamma + ik + \mu_S)(\gamma + \mu_a) = 1. \tag{C1}$$

The solution is then given by means of the Fourier transform

$$E_{S,a}(x,t) = \int_{-\infty+i\sigma}^{\infty+i\sigma} \tilde{E}_{S,a}(k) \exp(-ikx) \exp[\gamma(k)t]\, dk,$$

where k is a complex number, and

$$\tilde{E}_{S,a}(k) = \int_{-\infty}^{\infty} E_{S,a}(x,t=0) \exp(ikx)\, dx.$$

Looking for backward-traveling waves with velocity V,

$$z = x + Vt,$$

the solution is written

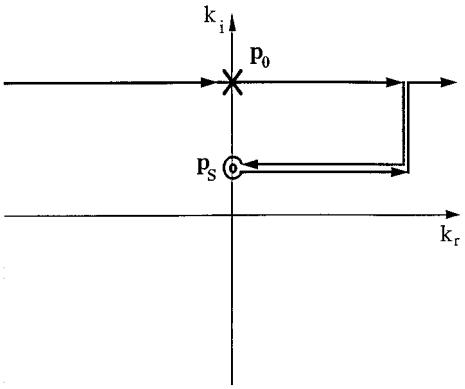

FIG. 14. Contour in the complex k plane.

$$E_{S,a}(z,t)=\int_{-\infty+i\sigma}^{\infty+i\sigma}\widetilde{E}_{S,a}(k)\exp[\gamma(k)+ikV]t\ \exp[-ikz]dk, \tag{C2}$$

where $\widetilde{E}_{S,a}(k)$ is the Fourier transform of the initial condition. This linear solution holds for long times t, allowing us to obtain the asymptotic behavior of the far wave front of the pulse. In order to compute this integral, we remark, on the one hand, that the real part of the function $f(k)=\gamma(k)+ikV$ has a saddle point at $k_0=ip_0$ (p_0 being real) that is maximum along the real k axis and minimum along the imaginary axis. On the other hand, because of the exponential wave-front dependence $E_{S,a}(x)\propto\exp(p_s x)$, the corresponding Fourier transform $\widetilde{E}_{S,a}(k)$ has a pole at $k_s=ip_s$ (p_s being real). Two cases must be then analyzed.

(a) $p_s<p_0$: The contour in the complex k plane, which may be chosen, is shown in Fig. 14; therefore, for long-time interaction, the integral (C2) can be written as the sum of the pole and the saddle-point contributions,

$$E_{S,a}(z,t)=I_{\rm pol}+I_{\rm sad},$$

with

$$I_{\rm pol}\propto\widetilde{E}_{S,a}(k=ip_s)\exp[f(k=ip_s)t]\exp(p_s z),$$

and

$$I_{\rm sad}\propto(tf''_{p=p_0})^{-1/2}\widetilde{E}_{S,a}(k=ip_0)\exp[f(k=ip_0)t]\exp(p_0 z).$$

Since the real part of the function $f(k)$ has a minimum along the imaginary axis, the long-time behavior will be dominated by the pole. The corresponding stationary condition is then written

$$V(k)=i\frac{\gamma(k)}{k}, \tag{C3}$$

which describes a continuous family of stable solitary structures whose velocity (Fig. 10) is only dependent on the wave front slope p_s.

(b) $p_s>p_0$: In this case, the pole can no more contribute to the integral since all the singularities must lie inside the upper half-plane contour. Following the steepest descent method [22], the supplementary condition is

$$V=[\partial\gamma(k)/\partial k]_{k=k_0};$$

the velocity and the head-front slope then become fixed by (C1) and (C3),

$$V_0=\frac{2+\mu_a^2-\mu_S\mu_a+2\sqrt{1-\mu_S\mu_a}}{4+(\mu_a-\mu_S)^2},$$

$$p_0=\frac{1}{\mu_S}+\mu_S-\frac{1}{\mu_a}-\mu_a+\frac{\sqrt{1-\mu_S\mu_a}}{\mu_a}+\frac{\sqrt{1-\mu_S\mu_a}}{\mu_S}.$$

Any initial slope condition $p_S>p_0$ spreads until reaching the minimum point attractor p_0.

[1] D. Pohl and W. Kaiser, Phys. Rev. B **1**, 31 (1970).

[2] V. A. Gorbunov, S. B. Papernyi, and V. R. Startsev, Kvant. Elektron. (Moscow) **10**, 1386 (1983) [Sov. J. Quantum Electron **13**, 900 (1983)].

[3] B. Gellert and B. Kronast, Appl. Phys. B **32**, 175 (1983); **33**, 29 (1984).

[4] J. Botineau, C. Leycuras, C. Montes, and E. Picholle, J. Opt. Soc. Am. B **6**, 300 (1989).

[5] E. Picholle, C. Montes, C. Leycuras, O. Legrand, and J. Botineau, Phys. Rev. Lett. **66**, 1454 (1991).

[6] C. Montes, A. Mamhoud, and E. Picholle, Phys. Rev. A **49**, 1344 (1994).

[7] M. Maier, W. Kaiser, and J. A. Giordmaine, Phys. Rev. Lett. **17**, 1275 (1966).

[8] S. A. Arrivo, K. G. Spears, and J. Sipior, Opt. Commun. **116**, 377 (1995).

[9] J. Coste and C. Montes, Phys. Rev. A **34**, 3940 (1986).

[10] C. Montes, A. Mikhailov, A. Picozzi, and F. Ginovart, preceding paper, Phys. Rev. E **55**, 1086 (1997).

[11] S. C. Chiu, J. Math. Phys. **19**, 168 (1978).

[12] Superluminous motion of the three-wave localized structure does not contradict by any means the special theory of relativity. This motion can be viewed as the result of the convective amplification of the leading edges of the Stokes and material pulses, whereas their rears are attenuated, the pump wave being depleted during the interaction and totally or partially restored after that. No transportation of information can be obtained *via* this deformation process which can only occur if a sufficiently extended background of Stokes light is available.

[13] J. A. Armstrong, S. S. Jha, and N. S. Shiren, IEEE J. Quantum. Electron. **QE-6**, 123 (1970).

[14] K. Nozaki and T. Taniuti, J. Phys. Soc. Jpn. **34**, 796 (1973); Y. Oshawa and K. Nozaki, *ibid.* **36**, 591 (1974).

[15] S. F. Morosov, L. V. Piskunova, M. M. Sushik, and G. I. Freidman, Kvant. Elektron. (Moscow) **5**, 1005 (1978) [Sov. J. Quantum. Electron. **8**, 576 (1978)].

[16] E. Gaizauskas and K. Staliunas, Opt. Commun. **114**, 463 (1995).

[17] D. J. Kaup, J. Nonlinear Sci. **3**, 427 (1993).
[18] A. Hasegawa, in *Optical Solitons in Fibers* (Springer-Verlag, Berlin, 1990).
[19] V. G. Kolmogorov, I. G. Petrovskii, and N. S. Piskunov, Bull. Moscow State Univ. Math. Mech. **1**, 1 (1937).
[20] D. J. Kaup, A. Reiman, and A. Bers, Rev. Mod. Phys. **51**, 275 (1979).
[21] C. Montes and O. Legrand, in *Electromagnetic and Acoustic Scattering: Detection and Inverse Problem* (World Scientific, Singapore, 1989) pp. 209–221; O. Legrand and C. Montes, J. Phys. (Paris) Colloq. **50**, C3-147 (1989).
[22] Ph. M. Morse and H. Feshbach, in *Methods of Theoretical Physics* (McGraw-Hill, New York, 1953), p. 437.